Journal of Power Sources 242 (2013) 349–356

Contents lists available at SciVerse ScienceDirect

Journal of Power Sources

journal homepage: www.elsevier.com/locate/jpowsour

Investigation of the effect of shunt current on battery efficiency and stack temperature in vanadium redox flow battery

Ao Tang, John McCann, Jie Bao, Maria Skyllas-Kazacos*

School of Chemical Engineering, University of New South Wales, Sydney, New South Wales 2052, Australia

HIGHLIGHTS

- Shunt currents in VFB deteriorate battery performance.
- Thermal effect of shunt currents needs to be considered during standby.
- A complete model can predict battery efficiencies and electrolyte temperature in open circuit.
- The trade-off between shunt loss and pumping consumption needs to be considered.
- Temperature control system can be developed to manage the electrolyte temperature on the basis of a complete model.

ARTICLE INFO

Article history:
Received 11 April 2013
Received in revised form
17 May 2013
Accepted 19 May 2013
Available online 4 June 2013

Keywords:
Vanadium redox flow battery
Shunt current
Stack efficiency
Stack temperature in open-circuit

ABSTRACT

In vanadium redox flow batteries (VFB), the power of the battery is determined by the number of cells in the stack. Serial and parallel layouts are commonly adopted interactively to suit the designed power demand. The bipolar stack design inevitably introduces shunt currents bypassing into the common manifolds in the stack and thereby resulting in a parasitic loss of power and energy. During standby, shunt current and its associated internal discharge reactions can generate heat and increase stack temperature, potentially leading to thermal precipitation in the positive half-cell. This study aims to investigate the effect of shunt current on stack efficiency and temperature variation during standby periods for a 40-cell stack. Dynamic models based on mass balance, energy balance and electrical circuit are developed for simulations and the results provide an insight into stack performance that will aid in optimising stack design and suitable cooling strategies for the VFB.

1. Introduction

Redox flow battery systems are regarded as one of the most promising energy storage devices that allow energy to be stored in separate reservoirs, providing in practice, flexibility in design of output power and storage capacity for specific installations with certain requirements. Successful testing and demonstrations in both laboratory and industrial installations ranging from a few kW/kWh to several MW/MWh systems have been reported over the past few decades, spanning the areas of load levelling, peak shaving, emergency back-up systems and particularly in combination with renewable energy sources such as wind and solar [1,2].

Of all the redox flow battery systems to date, the all-vanadium redox flow battery (VFB) has exhibited the greatest potential for large energy storage with its advantages of low capital cost, long life cycle, high energy efficiency and low-toxicity. The VFB has been developed for almost three decades and has also become one of the few flow batteries that have reached commercial fruition. Companies in China, Japan, Austria, the United States and the UK are currently manufacturing VFB products and installing them in both grid-connected and off-grid industrial and commercial projects. Research by numerous groups around the world is ongoing and primarily aimed at improving VFB efficiency, reducing cost and developing new generation VFBs [3–7].

The University of New South Wales (UNSW) has played a key role in the field of VFB research and engaged in VFB development for over 28 years that can be dated back to 1980s when Skyllas-Kazacos and co-workers were the first to successfully demonstrate the use of vanadium redox couples in both half-cell electrolytes for an all-vanadium redox flow battery [8–11]. Subsequent development programs at UNSW covered a wide range of projects from basic electrochemical and material research to advanced monitoring and control studies [12,13]. These were accompanied by several field trials of the VFB by the UNSW group, including an

* Corresponding author. Tel.: +61 2 9385 4335; fax: +61 2 9385 5966.
E-mail address: m.kazacos@unsw.edu.au (M. Skyllas-Kazacos).

0378-7753/$ – see front matter © 2013 Elsevier B.V. All rights reserved.
http://dx.doi.org/10.1016/j.jpowsour.2013.05.079

Nomenclature

A	surface area (m^2)
C_p	specific heat ($J\ g^{-1}\ K^{-1}$)
c	vanadium concentration ($mol\ L^{-1}$)
d	membrane thickness (m)
F	Faraday's constant ($C\ mol^{-1}$)
H	change of enthalpy ($J\ mol^{-1}$)
I	current (A)
k	diffusion coefficient ($m^2\ s^{-1}$)
num	number of cells
Q	flow rate ($L\ s^{-1}$)
R	resistance (Ω)
R_0	gas constant ($J\ mol^{-1}\ K^{-1}$)
S	electrode area (m^2)
T	temperature (°C)
U	overall heat transfer coefficient ($W\ m^{-2}\ K^{-1}$)
V	volume (L)
z	electrons involved in the redox reaction

Greek symbol

ρ	electrolyte density ($g\ L^{-1}$) ,

Superscript

cell	cell
tank	tank

Subscript

(10)	self-discharge reaction (10)
(11)	self-discharge reaction (11)
(13)	self-discharge reaction (13)
(14)	self-discharge reaction (14)
2	V^{2+}
3	V^{3+}
4	VO^{2+}
5	VO_2^+
air	surrounding air
−	negative side
+	positive side
stack	stack

electric golf cart and the first VFB Powered Solar Demonstration House in Thailand in the mid-1990s. Recent activities being undertaken at UNSW involve VFB installations on campus in combination with a wind turbine and solar panel for the purpose of providing off-grid power supply and load levelling.

The unique and competitive features of the VFB compared to other flow batteries are associated with long cycle life and high energy efficiencies. As with all flow battery systems, efficiency is linked to good stack design and operation. In the case of bipolar stacks, the inherent existence of shunt currents can influence battery performance. This is predominantly revealed in large power stack configurations where a number of individual cells are connected in series with common electrolyte manifolds. Unlike other types of flow batteries such as the zinc-bromine battery in which corrosion and deposition may occur at electrodes as a result of shunt current, vanadium redox flow battery systems merely suffer from power loss in stack performance, this being one of the advantages of eliminating metal plating and having the same species in both half cells. For good energy efficiency and thermal management however, shunt current minimisation is important.

Articles on shunt current modelling in flow batteries can be found in the literature dating back to the 1970s starting from early work by researchers at NASA [14–26]. Despite a great deal of research being undertaken, however, none of the previous work has considered the overall stack efficiency spanning the whole operating state-of-charge with a complete dynamic model. In addition, the thermal effect of shunt current on stack temperature has been also neglected.

Previous models account for the bypass currents that flow through the electrolyte manifolds during charging and discharging, but these do not explain the internal discharge processes that occur through the manifolds during periods of standby when the pumps are switched off. These bypass currents have traditionally been suppressed in Zn/Br systems by draining the electrolyte manifolds during standby periods to avoid excessive internal heating and capacity loss. Self-discharge processes resulting from diffusion of vanadium ions across the membrane during standby periods have already been modelled [27], however, shunt current along with its associated internal discharge, has, to our knowledge, so far been ignored. In fact, the thermal effects of shunt current and its associated internal discharge on electrolyte temperature are negligible in comparison to ohmic loss from cell resistances in charging and discharging. During standby periods, however, when combined with the effect of self-discharge through the membrane, considerable heat could be generated which could dramatically increase the stack temperature, thereby potentially inducing precipitation of VO_2^+ and blocking the cell channels in the stack.

This paper aims to investigate the effect of shunt current on stack performance and its thermal effect on stack temperature variation during standby conditions for a 5 kW stack comprising 40 individual cells. The round-trip efficiency under different charging-discharging currents is calculated dynamically by combining the mass balance with the electrical circuit of shunt current, in which the loss of efficiency resulting from the vanadium ion diffusion is considered as well. Ohmic loss from shunt current along with its associated internal discharge heat in the stack at open-circuit is also considered and simulated. The results provide an insight into the maximum stack electrolyte temperature that could be potentially reached during standby periods with the stack at open-circuit and will assist in optimising stack design, and appropriate cooling strategies for the development of an advanced temperature control system.

2. Dynamic modelling of the VFB

2.1. Modelling of shunt current

Modelling studies of shunt current in flow batteries were initiated by NASA in 1970s [14–16], followed by a number of modified models in the literature [17–26], most of which employ an electrical circuit analogy to describe the bypassing flow of current in a bipolar stack with common electrolyte manifolds. A typical electrical circuit diagram of shunt current in the stack of the VFB is displayed in Fig. 1, where the voltage source V is the cell voltage and R is the cell resistance. The subscripts of m, c and i represent the manifold, channel and cell respectively, while the superscripts of + and − stand for the positive and negative half cells.

The resistance of the cell can be determined experimentally, and the ionic resistances of channel and manifold are calculated on the basis of specific flow-frame design and electrolyte conductivity determined according to Eq. (1):

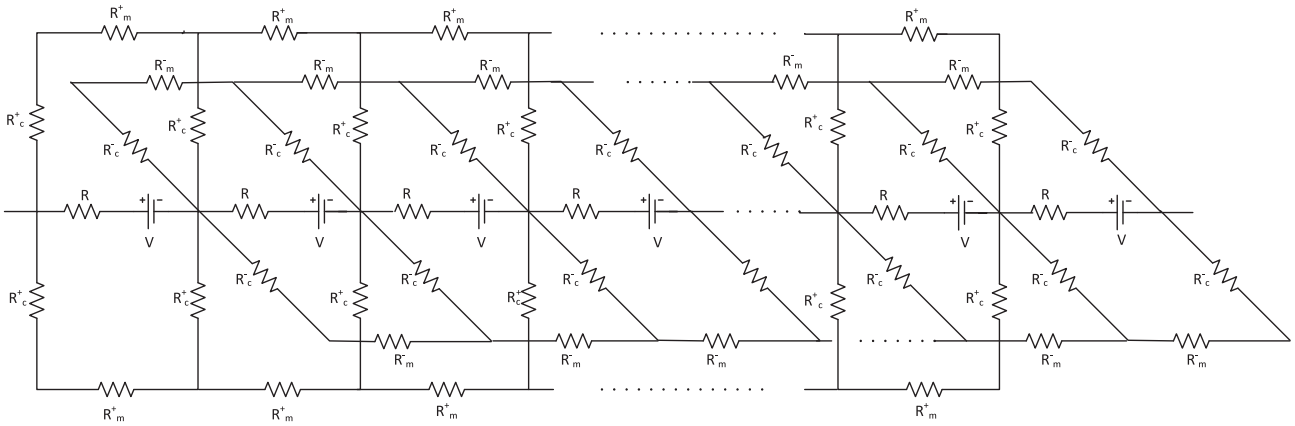

Fig. 1. Electrical circuit analogy of a bipolar stack.

$$R = \frac{1}{\sigma}\frac{l}{S} \tag{1}$$

where l is the length, S is the cross-sectional area and σ is the electrolyte conductivity which is a function of SOC. Applying Kirchhoff's current and voltage laws to the electrical circuit along with mesh current analysis [28], the magnitude and direction of currents flowing through each resistor can be calculated.

2.2. Mass balance and dynamic model

The electrical circuit model of shunt current can be used to predict the internal currents at a given state-of-charge. By combining mass balance equations with the electrical model, a complete dynamic model can be developed to study the battery during charging and discharging. Some assumptions were made for the development of the model:

(1) The concentration in each tank and cell (or stack) is uniform.
(2) The electrolyte is fully filled in the tank.
(3) Self-discharge reactions through the membrane are instantaneous.
(4) The effects of side reactions due to vanadium ion diffusion described in Eqs. (12) and (15) are negligible.
(5) The stack and tanks behave as continuous stirred tank reactors (CSTRs).
(6) Cell resistance remains constant over the operating state-of-charge range;
(7) Gassing side reactions are negligible.

Each of the four different oxidation states of the vanadium ion can be modelled for the tank and the individual cells in the stack on the basis of conversion of mass as follows [11]. In the tank

$$V^{\text{tank}}\frac{\mathrm{d}c_2^{\text{tank}}}{\mathrm{d}t} = Q\left(c_2^{\text{cell }1} + c_2^{\text{cell }2} + \cdots + c_2^{\text{cell }n}\right) - \text{num}\cdot Qc_2^{\text{tank}} \tag{2}$$

$$V^{\text{tank}}\frac{\mathrm{d}c_3^{\text{tank}}}{\mathrm{d}t} = Q\left(c_3^{\text{cell }1} + c_3^{\text{cell }2} + \cdots + c_3^{\text{cell }n}\right) - \text{num}\cdot Qc_3^{\text{tank}} \tag{3}$$

$$V^{\text{tank}}\frac{\mathrm{d}c_4^{\text{tank}}}{\mathrm{d}t} = Q\left(c_4^{\text{cell }1} + c_4^{\text{cell }2} + \cdots + c_4^{\text{cell }n}\right) - \text{num}\cdot Qc_4^{\text{tank}} \tag{4}$$

$$V^{\text{tank}}\frac{\mathrm{d}c_5^{\text{tank}}}{\mathrm{d}t} = Q\left(c_5^{\text{cell }1} + c_5^{\text{cell }2} + \cdots + c_5^{\text{cell }n}\right) - \text{num}\cdot Qc_5^{\text{tank}} \tag{5}$$

In each individual cell

$$\frac{V^{\text{cell}}}{2}\frac{\mathrm{d}c_2^{\text{cell }n}}{\mathrm{d}t} = Q\left(c_2^{\text{tank}} - c_2^{\text{cell }n}\right) \pm \frac{I^{\text{cell }n}}{zF} - k_2\frac{c_2^{\text{cell }n}}{d}S - 2k_5\frac{c_5^{\text{cell }n}}{d}S - k_4\frac{c_4^{\text{cell }n}}{d}S \tag{6}$$

$$\frac{V^{\text{cell}}}{2}\frac{\mathrm{d}c_3^{\text{cell }n}}{\mathrm{d}t} = Q\left(c_3^{\text{tank}} - c_3^{\text{cell }n}\right) \mp \frac{I^{\text{cell }n}}{zF} - k_3\frac{c_3^{\text{cell }n}}{d}S + 3k_5\frac{c_5^{\text{cell }n}}{d}S + 2k_4\frac{c_4^{\text{cell }n}}{d}S \tag{7}$$

$$\frac{V^{\text{cell}}}{2}\frac{\mathrm{d}c_4^{\text{cell }n}}{\mathrm{d}t} = Q\left(c_4^{\text{tank}} - c_4^{\text{cell }n}\right) \mp \frac{I^{\text{cell }n}}{zF} - k_4\frac{c_4^{\text{cell }n}}{d}S + 3k_2\frac{c_2^{\text{cell }n}}{d}S + 2k_3\frac{c_3^{\text{cell }n}}{d}S \tag{8}$$

$$\frac{V^{\text{cell}}}{2}\frac{\mathrm{d}c_5^{\text{cell }n}}{\mathrm{d}t} = Q\left(c_5^{\text{tank}} - c_5^{\text{cell }n}\right) \pm \frac{I^{\text{cell }n}}{zF} - k_5\frac{c_5^{\text{cell }n}}{d}S - 2k_2\frac{c_2^{\text{cell }n}}{d}S - k_3\frac{c_3^{\text{cell }n}}{d}S \tag{9}$$

where vanadium ion diffusion is modelled by Fick's law and the following side reactions that occur in the cell., In the positive cells, the diffusion of V^{2+} and V^{3+} ions leads to

$$V^{2+} + 2VO_2^+ + 2H^+ \rightarrow 3VO^{2+} + H_2O \tag{10}$$

$$V^{3+} + VO_2^+ \rightarrow 2VO^{2+} \tag{11}$$

$$V^{2+} + VO^{2+} + 2H^+ \rightarrow 2V^{3+} + H_2O \tag{12}$$

In the negative cells, the diffusion of VO^{2+} and VO2$^+$ ions lead to

$$VO^{2+} + V^{2+} + 2H^+ \rightarrow 2V^{3+} + H_2O \tag{13}$$

$$VO_2^+ + 2V^{2+} + 4H^+ \rightarrow 3V^{3+} + 2H_2O \tag{14}$$

$$VO_2^+ + V^{3+} \rightarrow 2VO^{2+} \tag{15}$$

In order to link the mass balance to the electrical circuit model of shunt current, the Nernst equation is employed to calculate the

open-circuit cell voltage of each cell at a given state-of-charge on the basis of vanadium concentration in each half-cell.

$$E_{\text{cell}} = E^{'} + \frac{RT}{zF} \ln\left(\frac{\left[V^{2+}\right]\left[VO_2^{+}\right]}{\left[V^{3+}\right]\left[VO^{2+}\right]}\right) \tag{16}$$

where $E^{'}$ is formal potential, R is the universal gas constant, T is the temperature in °K, F is Faraday's constant, and z is the number of equivalents transferred per mole of reduced or oxidized species. Once the open-circuit voltages and electrolyte resistances have been ascertained, the internal cell currents can be determined from the shunt current model depicted in Fig. 1 and fed back to the mass balance equations for the purpose of dynamic prediction.

2.3. Simulation conditions and results

2.3.1. VFB stack parameters

The specification of the VFB and the parameters employed in the present simulation are listed in Table 1. The 5 kW/15 kWh VFB used in this simulation is based on an early UNSW prototype stack consisting of 40 individual cells and 200 L of 2 M vanadium in 5 M total sulphate solution in each half-cell reservoir. For the purpose of this study, Selemion CMV membranes are employed to separate the two half-cell solutions, and the corresponding vanadium ion diffusion coefficients are assumed to be temperature independent. It is also assumed that the average cell resistivity during operation is constant with a value of 2.1 Ω cm^2. The flow frame of the stack is assumed to be made of polypropylene with an edge width of 3.5 cm. The end plates are assumed to be covered by stainless steel, where the thicknesses of inner polypropylene layer and outer steel layer are 2 cm and 1 cm respectively. The detailed stack parameters are listed in Table 1.

Table 1
Specifications of the VFB and parameters in the simulation [27,29].

Parameters	Value
Total vanadium concentration	2 mol L^{-1}
Dimension of each cell	50 cm × 30 cm × 0.6 cm
Number of cells, num	40
Membrane area, S	1500 cm^2
Faraday's constant, F	96,485 C mol^{-1}
Number of electrons transferred, z	1
Diffusion coefficient of V^{2+}, k_2	3.17×10^{-8} m s^{-1} (25 °C)
Diffusion coefficient of V^{3+}, k_3	7.16×10^{-9} m s^{-1} (25 °C)
Diffusion coefficient of VO^{2+}, k_4	2×10^{-8} m s^{-1} (25 °C)
Diffusion coefficient of VO_2^{+}, k_5	1.25×10^{-8} m s^{-1} (25 °C)
Cell volume, V^{cell}	0.9 L
Tank volume, V^{tank}	200 L per reservoir
Formal potential, E_0	1.4 V
Specific heat capacity of electrolyte, C_p	3.2 J g^{-1} K^{-1}
Electrolyte density, ρ	1.354 g cm^{-3}
Enthalpy change of discharge reaction at positive side, ΔH_+	−122.8 kJ mol^{-1}
Enthalpy change of discharge reaction at negative side, ΔH_-	−33 kJ mol^{-1}
Enthalpy change of side reaction (10), $\Delta H_{(10)}$	−220 kJ mol^{-1}
Enthalpy change of side reaction (11), $\Delta H_{(11)}$	−64 kJ mol^{-1}
Enthalpy change of side reaction (13), $\Delta H_{(13)}$	−91.2 kJ mol^{-1}
Enthalpy change of side reaction (14), $\Delta H_{(14)}$	−246.8 kJ mol^{-1}
Ratio of channel length to cross-sectional area	833.3 cm^{-1}
Ratio of manifold length (each cell) to cross-sectional area	0.085 cm^{-1}
Average cell resistivity, R_i	2.1 Ω cm^2
Thickness of flow frame	3.5 cm
Thermal conductivity of polypropylene	0.16 W m^{-1} K^{-1}
Overall heat transfer capability of the stack, $U_s \times A_s$	1.77 J K^{-1} s^{-1}

To be able to obtain the channel and manifold resistances as shown in Eq. (1), the electrolyte conductivity which is a function of SOC or concentration needs to be known. The following relations derived from experimental data were used to determine the electrolyte conductivity [30]:

$$\sigma_+ = 235 + 46.43 * c_5^{\text{tank}} \tag{17}$$

$$\sigma_- = 160 + 30.5 * c_2^{\text{tank}} \tag{18}$$

where c_5^{tank} and c_2^{tank} represent the concentration of VO_2^+ and V^{2+} ions in the positive and negative half-cell reservoirs respectively as a function of SOC. The range of operating SOC was assumed to be from 10% to 90% and employed in the simulation. The flow rate was set to be twice that of the theoretical flow rate required to reach 10% SOC during discharge and 90% SOC during charging derived from Faraday's law and was kept constant during the operation. Due to the imbalance of SOC induced by vanadium ion diffusion, however, the tank concentrations of V^{2+} and VO_2^+ ions were used as indicators to cease the charging and discharging instead of the SOC limits.

2.3.2. Simulation results

To start with, the battery is charged and discharged at 60 A from 10% to 90% SOC indicated by the tank concentration of V^{2+} or VO_2^+. Fig. 2 shows the case of charging, while Fig. 3 reveals the changes in cell voltage, internal currents, ion concentrations and resistances as a function of time during discharging. It can be observed that due to the existence of large channel resistance for the present flow-frame design, shunt current only accounts for a small portion of the loss of cell currents and therefore the imbalances in internal cell currents and cell voltages will not result in a large loss of efficiency. The charging time and discharging time were determined as 4.2 h and 4.04 h respectively and the round-trip coulombic efficiency was calculated as 95.5%. By assuming no vanadium ion diffusion existed, a round-trip coulombic efficiency of 99% was determined, which means that shunt current loss only accounts for 1% loss of the total coulombic efficiency, while the rest of the coulombic efficiency loss arises from vanadium ion diffusion and side reactions.

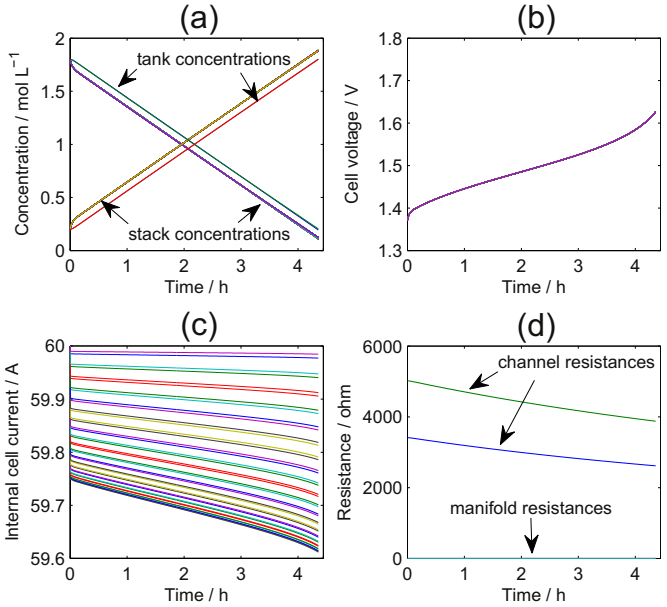

Fig. 2. Charging profiles at 60 A.

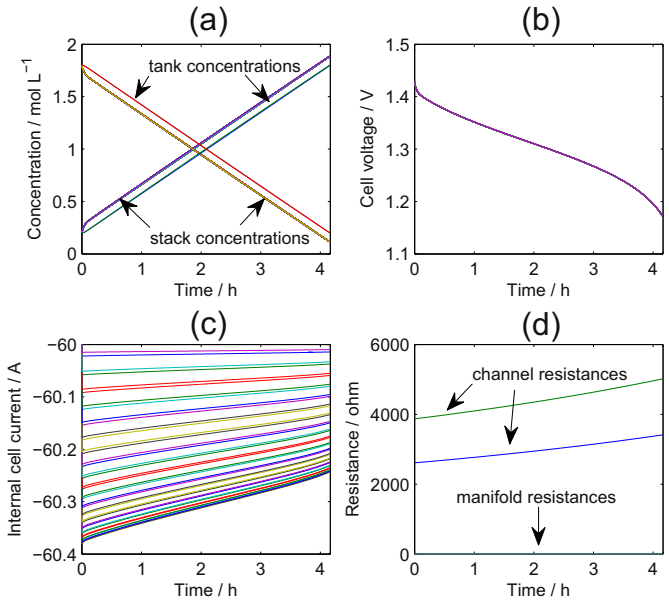

Fig. 3. Discharge profiles at 60 A

By varying the discharging currents, coulombic efficiency at any discharging current can be calculated based on the simulation results. In addition to coulombic efficiency, voltage efficiency, defined as the ratio of average discharging cell voltage to average charging cell voltage, and energy efficiency can be also determined from simulations. Fig. 4 shows the stack efficiencies as a function of discharging current with a 60 A charging current. The coulombic efficiency is observed to increase with increasing discharging current, while voltage efficiency decreases except at a small discharging current of 1 A. This trend is caused by the slow vanadium ion diffusion across the membrane and a large IR drop at fast discharging rates respectively. Moreover, the energy efficiency reaches a peak of 83.8% at 40 A discharging current. Stack efficiencies versus discharging current at charging currents of 40 A, 60 A, 80 A and 100 A are summarized in Fig. 5, in which the energy efficiency of the stack is seen to reach 85%. These results are consistent with experimental stack performance curves published in the literature [4].

In order to highlight the importance of stack design for good stack performance, additional simulations were carried out for a less than optimised flow-frame design. For the purpose of comparison, the channel resistances were reduced to one fifteenth of the original values representing a typical poor flow-frame design with short channels and/or a large manifold diameter. Fig. 6 depicts the variation in resistances and corresponding internal charging cell currents at 60 A, while Fig. 7 shows the stack efficiencies at different discharging currents. These results demonstrate that both coulombic and energy efficiencies decrease notably with the large shunt currents during charging and discharging due to the improper flow-frame design that facilitates ionic current bypassing. As seen from the above simulation results, the complete dynamic model can aid in the visualization of variations in key parameters of the VFB under certain circumstances and provide information which will assist the design of flow frames and stacks to achieve a required performance in terms of energy efficiency. Of equal importance however, is the thermal effect of bypassing currents on stack temperature, particularly when the pumps are switched off during standby.

3. Thermal effect in open-circuit

3.1. Thermal modelling of the stack

A previous study has demonstrated a significant thermal effect on stack temperature at open-circuit [27] as a result of ions diffusing across the membrane and generating heat from the resultant self-discharge reactions. By further considering both ohmic dissipation and internal discharge heat from shunt currents determined from the electrical circuit model of Fig. 1, however, a complete thermal model for the open-circuit case is developed on the basis of the energy balance as shown in Eq. (19):

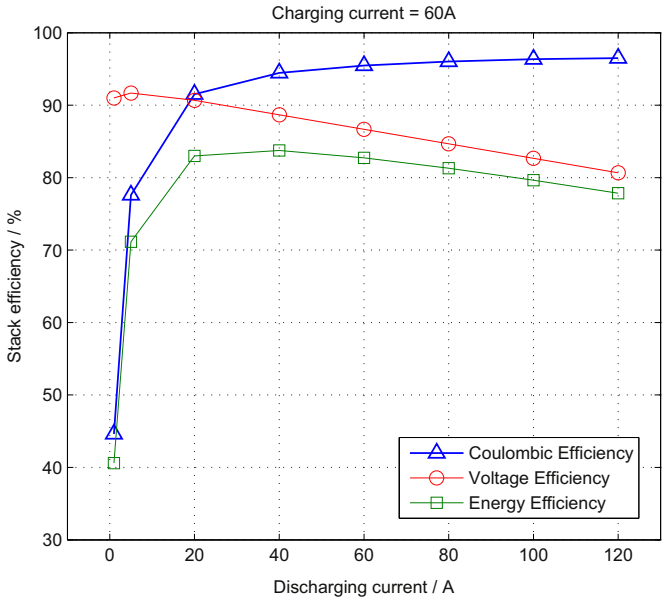

Fig. 4. Stack efficiencies at different discharging currents with 60 A charging current.

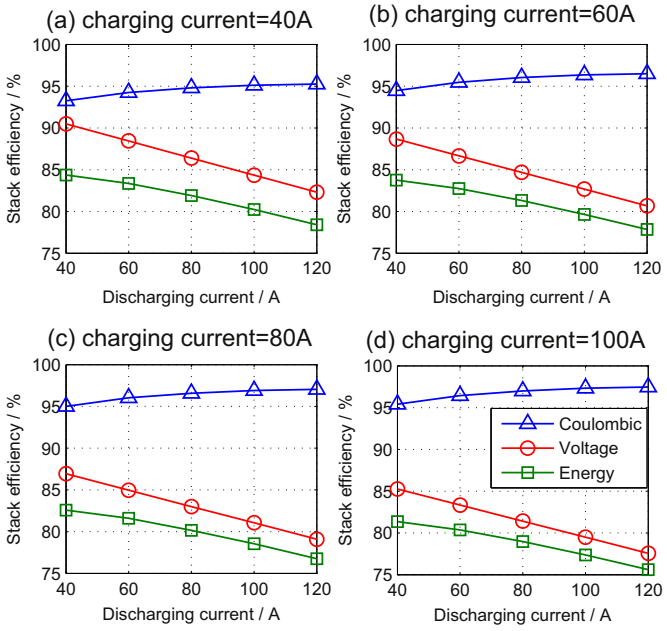

Fig. 5. Stack efficiencies versus discharging current at different charging currents.

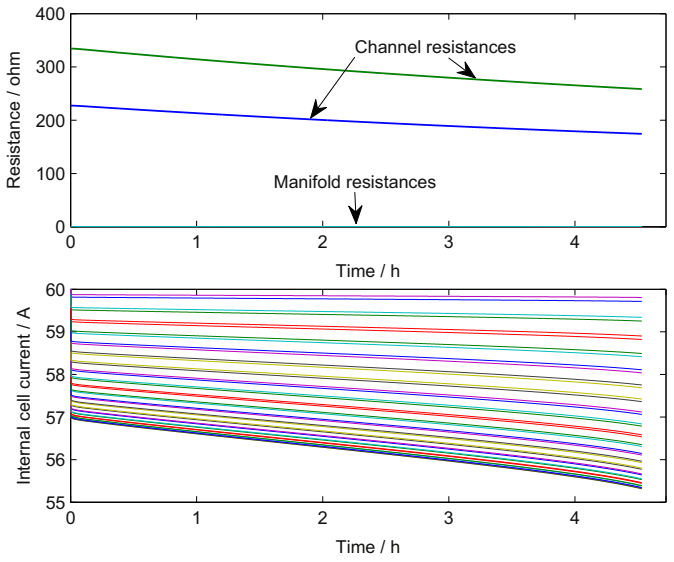

Fig. 6. Resistance and internal cell current vs. time at 60 A charging with a poor flow-frame design.

$$\rho C_p V_{stack}\frac{dT_{stack}}{dt} = U_s A_s(T_{air} - T_{stack}) + \text{num}\cdot k_2\frac{c_2^s}{d}S(-\Delta H_1) + \text{num}\cdot k_3\frac{c_3^s}{d}S(-\Delta H_2) + \text{num}\cdot k_4\frac{c_4^s}{d}S(-\Delta H_4) + \text{num}\cdot k_5\frac{c_5^s}{d}S(-\Delta H_5) + I^2R + \frac{I_{id}}{zF}(-\Delta H_+ - \Delta H_-) \quad (19)$$

where I^2R accounts for the total ohmic loss through each channel, manifold and cell in the stack; I_{id} is sum of the internal discharge currents associated with the shunt current; ΔH_+ and ΔH_- are the changes of enthalpy for discharge reactions at positive side and negative side respectively; c_2^s, c_3^s, c_4^s and c_5^s are the average stack concentrations of V^{2+}, V^{3+} ,VO^{2+} and VO_2^+ that can be obtained from the mass balance model.

Together with the mass balance and electrical circuit model, the thermal model can predict the variation in stack temperature at open-circuit dynamically. Aside from the assumptions made for the mass balance in Section 2.2, the following assumptions were also made for the thermal model at open-circuit:

1) The temperature in the stack is uniform.
2) The Nernst equation is temperature dependent.
3) The thermal model is only valid when V^{2+} or VO_2^+ is not completely depleted in any single cell.

3.2. Simulation and results

The 5 kW/15 kWh VFB is investigated during standby periods. As the typical local night temperature varies from 5 °C to 15 °C depending on the season, it is assumed in the simulation that room temperature is constant at 10 °C. In addition, the initial stack electrolyte temperature is assumed to be 15 °C. With the above assumptions, simulations were carried out and the variations in stack temperature in the cases of both non-insulated and insulated stacks are provided in Figs. 8 and 9. It can be seen from Fig. 8 that the temperature in a non-insulated stack increases up to 40 °C after 16 h and will continue to rise until all of V^{2+} and VO_2^+ are completely depleted. By further considering the thermal effect of shunt current in the thermal model, it is predicted that the stack temperature will reach a higher temperature faster than for the case where only self-discharge heat associated with vanadium diffusion is generated. Fig. 9 compares the stack temperature variations in an insulated stack. Without heat exchange to the environment, the stack temperatures can soar up above 50 °C in both cases. Likewise, the stack temperature in the completed model reaches its maximum faster as a consequence of shunt current ohmic loss and associated internal discharge heat.

In Fig. 10, the variation in concentrations of vanadium ions in all 40 cells in open-circuit is shown. Due to the presence of shunt current, the centre cells are seen to undergo self-discharge faster than two end cells. This is also shown in Fig. 11, in which currents in channels, manifolds and cells at 50% SOC are indicated. As V^{2+} and VO_2^+ still exist in cells, the stack temperature will continue to

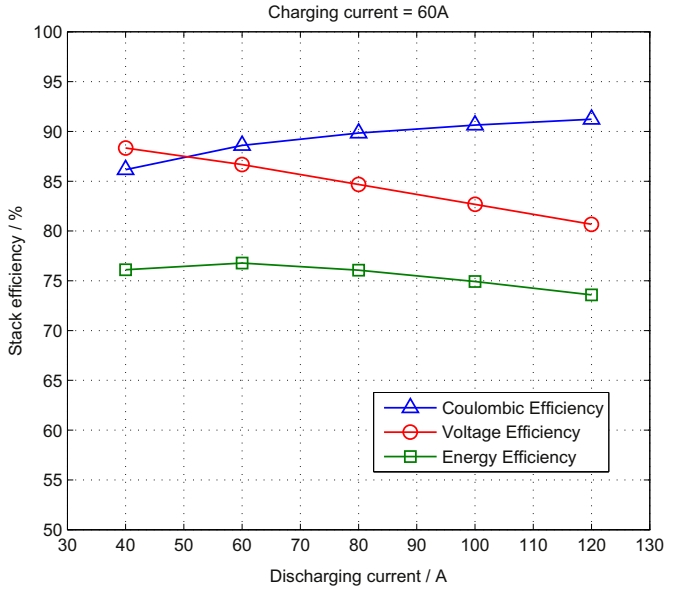

Fig. 7. Stack efficiencies at different discharging currents with 60 A charging current for a poor flow-frame design.

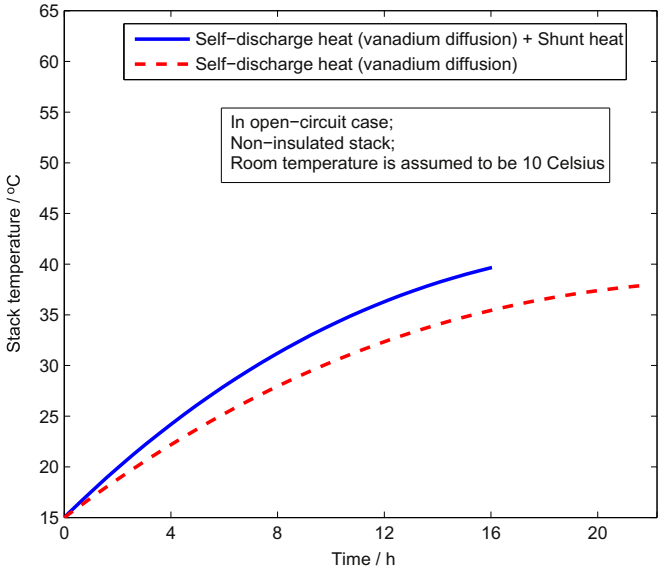

Fig. 8. Stack temperature variation at open-circuit with non-insulated stack.

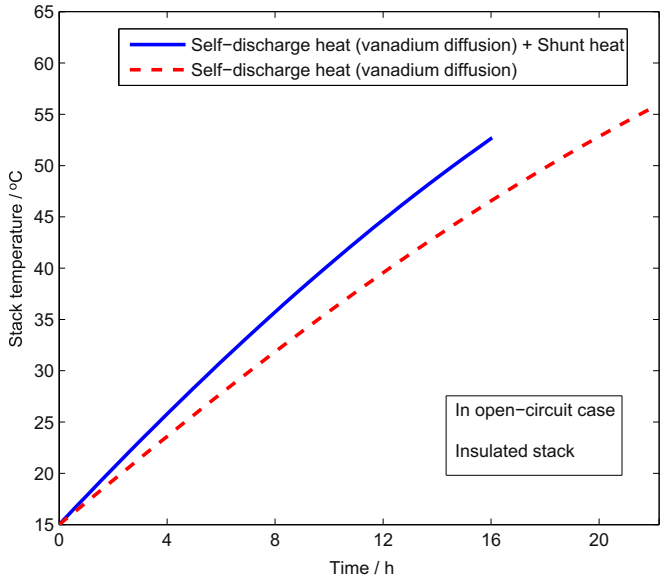

Fig. 9. Stack temperature variation at open-circuit with insulated stack.

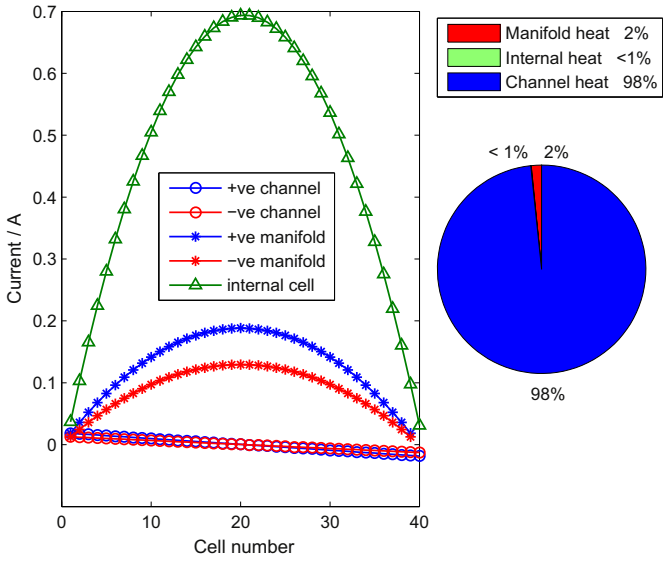

Fig. 11. Current distribution in the stack at 50% SOC (left) and pie graph showing relative contributions to ohmic dissipation at 50% SOC (right).

increase until V^{2+} and VO_2^+ are completely depleted in all individual cells. By comparing the cell temperatures in Figs. 8 and 9 with the VO_2^+ concentration profiles given in Fig. 10 however, it is possible to predict the VO_2^+ ion concentration at the time when the stack temperature reaches 40 °C and above where thermal precipitation of V_2O_5 could occur. Under the present design, it is expected that no thermal precipitation could occur due to the fact that the concentration of VO_2^+ will have dropped to a low level when the stack electrolyte temperature reaches 40 °C.

Fig. 11 also depicts the corresponding contribution to ohmic dissipation at 50% SOC in open-circuit, revealing that the heat from channel resistances to shunt currents play a dominant role in spite of very small current flowing through them in comparison with manifold and internal cell currents. This is due to the long length and small cross-sectional area of the channel in the flow-frame design that lead to the large ionic resistance observed in Fig. 2 or Fig. 3.

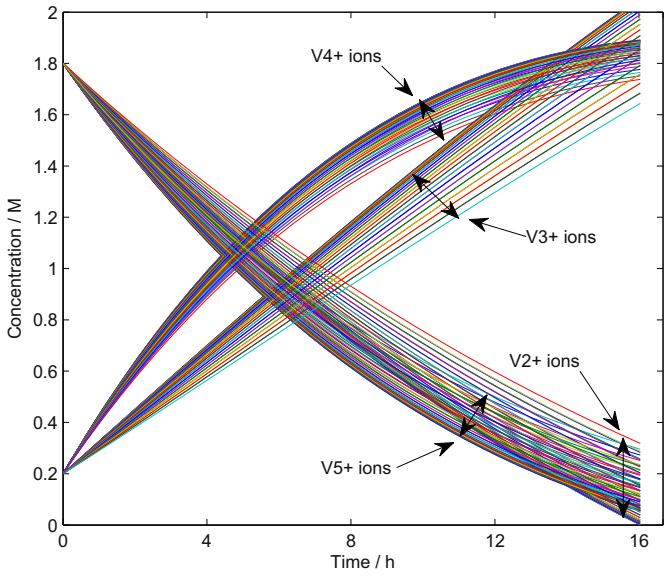

Fig. 10. Concentration variations caused by both self-discharge and shunt currents in all cells at open-circuit.

In addition to ohmic heat dissipation, both internal discharge and self-discharge heat also make contributions to the rise of stack temperature in open-circuit. Fig. 12 compares the three factors contributing to the heat released into the stack by both the rate of heat change and the proportions at 50% SOC. It is shown that for the present flow-frame design, self-discharge caused by the vanadium ion diffusion makes the greatest contribution to the increase in stack temperature amongst the three factors, while additive shunt current associated impacts (internal discharge and ohmic loss) on heat generation are also significant. The relative contributions of these factors can however change dramatically for a poor flow-frame design, further emphasising the need for shunt current reduction in bipolar stacks.

Using predictions of stack temperature from the complete thermal model in conjunction with a battery management system, control actions can be carried out to lower the stack temperature before it exceeds the VO_2^+ thermal precipitation point which will vary as a function of the composition of the electrolyte at open-circuit. This might be accomplished, for example, by restarting the pumping system for a short period to circulate the electrolyte

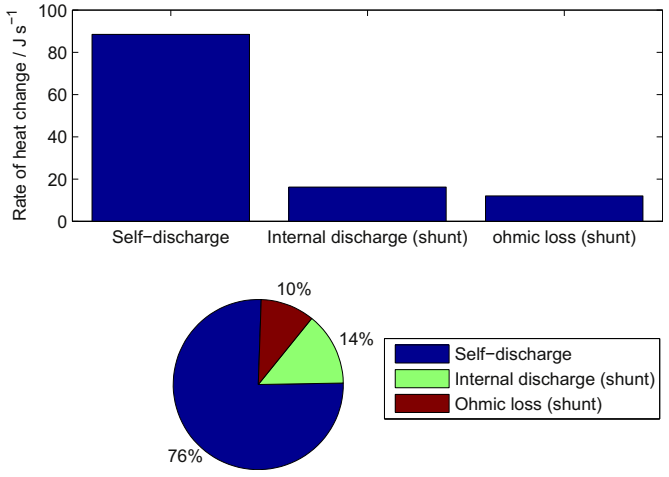

Fig. 12. Contribution to heat generation at 50% SOC.

between the tanks and stack. Furthermore, the complete thermal model has the potential to assist the design of an advanced temperature control system that will be able to assist in the cooling of the electrolyte in the electrolyte reservoirs when it is necessary during charging or discharging.

4. Conclusion

A complete dynamic model has been developed by combining shunt electrical circuit with mass balance equations. The proposed model uses mass balance equations for each individual cell and further considers the effects of shunt current on the redox reactions in a VFB, enabling more accurate predictions of concentration and cell voltage. Furthermore, it can also be used to predict stack efficiency under certain circumstances and provide an insight into battery design and optimisation. Based on this model, a complete thermal model is presented for open-circuit by further incorporating the thermal effect of shunt current into an earlier thermal model. Simulation results have shown that additional factors associated with shunt current can make signification contributions to the increase in stack temperature in open-circuit and a more accurate prediction of stack temperature can be acquired at given operating conditions. This thermal model may also be used to develop an electrolyte temperature control system for both continuous charging-discharging and standby periods, thereby avoiding thermal precipitation of V_2O_5 that could deposit on the positive electrode and block the channels and membranes and thus lower battery performance.

In order to reduce the effect of shunt current on stack efficiency and temperature, it is desirable to have longer length and smaller cross-sectional area channels. However, the longer the channels and the smaller their cross-sectional areas, the more pumping power will be required to circulate the electrolyte through the stack. As pumping systems are often driven by the battery itself, a trade-off between pumping power and shunt loss therefore needs to be considered in real VFB systems so that a maximum efficiency can be achieved with an optimal flow-frame design. Extended research on this issue is underway and will be reported in a separate paper.

References

[1] M. Skyllas-Kazacos, Encyclopedia of Electrochemical Power Sources, Elsevier, Amsterdam, 2009, pp. 444–453.
[2] R. L. Largent, M. Skyllas-Kazacos, J. Chieng, Proceedings of Twenty Third IEEE Photovoltaic Specialists Conference, Louisville, KY, USA (May 1993) 10–14.
[3] M. Skyllas-Kazacos, M.H. Chakrabarti, S.A. Hajimolana, F.S. Mjalli, M. Saleem, J. Electrochem. Soc. 158 (2011) R55–R79.
[4] M. Skyllas-Kazacos, G. Kazacos, G. Poon, H. Verseema, Int. J. Energy Res. 34 (2010) 182–189.
[5] Z. Yang, J. Zhang, M.C.W. Kintner-Meyer, X. Lu, D. Choi, J.P. Lemmon, J. Liu, Chem. Rev. 111 (2011) 3577–3613.
[6] G. Kear, A.A. Shah, F.C. Walsh, Int. J. Energy Res. 36 (2012) 1105–1120.
[7] W. Wang, Q. Luo, B. Li, X. Wei, L. Li, Z. Yang, Adv. Funct. Mater. 23 (2013) 970–986.
[8] M. Skyllas-Kazacos, M. Rychcik, R. Robins, All-vanadium redox battery, US Patent No. 4,786,567 (1988).
[9] M. Skyllas-Kazacos, M. Rychcik, R.G. Robins, A.G. Fane, M.A. Green, J. Electrochem. Soc. 133 (1986) 1057–1058.
[10] M. Skyllas-Kazacos, F. Grossmith, J. Electrochem. Soc. 134 (1987) 2950–2953.
[11] M. Rychcik, M. Skyllas-Kazacos, J. Power Sources 22 (1988) 59–67.
[12] A. Parasuraman, T.M. Lim, C. Menictas, M. Skyllas-Kazacos, Electrochim. Acta (2012). http://dx.doi.org/10.1016/j.electacta.2012.09.067.
[13] S. Corcuera, M. Skyllas-Kazacos, Eur. Chem. Bull. 1 (12) (2012) 511–519.
[14] P.R. Prokopius, NASA Technical Memorandum, NASA TM X-3359, April 1976.
[15] D.K. Stalnaker, A. Lieberman, NASA Technical Memorandum, NTIS Accession Number DE82000415, September 1981.
[16] N. Hagedorn, M.A. Hoberecht, L.H. Thaller, NASA Final report, "NASA redox cell stack shunt current, pumping power, and cell performance tradeoffs", NASA TM-82686, February 1982.
[17] E.A. Kominsky, R.F. Savinell, J. Electrochem. Soc. 130 (1983) 1103–1107.
[18] M. Yang, H. Wu, J.R. Selman, J. Appl. Electrochem. 19 (1989) 247–254.
[19] M. Zahn, G. Fla., P.G. Grimes, R.J. Bellows, United States patent, No. 4197169, 1980.
[20] R.E. White, C.W. Walton, H.S. Burney, R.N. Beaver, J. Electrochem. Soc. 133 (1986) 485–492.
[21] H.S. Burney, R.E. White, J. Electrochem. Soc. 135 (1988) 1609–1612.
[22] K. Kanarl, K. Nozaki, H. Kaneko, M. Kamimmoto, Proceedings of the Intersociety Energy Conversion Engineering Conference 3 (1990) 326–331.
[23] G. Codina, A. Aldaz, J. Appl. Electrochem. 22 (1992) 668–674.
[24] G. Codina, J.R. Perez, M. Lopez-Atalaya, J.L. Vazquez, A. Aldaz, J. Power Sources 48 (1994) 293–302.
[25] C.J. Gabriel, S. Szpak, J. Power Sources 25 (1989) 215–227.
[26] F. Xing, H. Zhang, X. Ma, J. Power Sources 196 (2011) 10753–10757.
[27] A. Tang, J. Bao, M. Skyllas-Kazacos, J. Power Sources 216 (2012) 489–501.
[28] M. Wang, Understandable Electric Circuits, Institution of Engineering and Technology, 2010.
[29] A. Tang, J. Bao, M. Skyllas-Kazacos, J. Power Sources 196 (2011) 10737–10747.
[30] M. Skyllas-Kazacos, M. Kazacos, J. Power Sources 196 (2011) 8822–8827.